

NONLINEAR OPTICAL PHENOMENA

PACS numbers: 42.70.Qs; 42.82.Gw; 42.50.Gy
DOI: 10.1070/QE2009v039n02ABEH013813

Effect of electromagnetically induced transparency on the spectrum of defect modes in a one-dimensional photonic crystal

V.G. Arkhipkin, S.A. Myslivets

***Abstract*. We studied the transmission spectrum of a one-dimensional photonic crystal containing a defect layer in which electromagnetically induced transparency is possible. The analysis is performed taking into account the spatial inhomogeneity of interacting fields in the photonic crystal. It is found that the transmission spectrum of such a photonic crystal depends on the spatial overlap of defect modes excited by probe and control radiations. It is shown that electromagnetically induced transparency can result in a considerable narrowing of the defect mode spectrum.**

Keywords: *photonic crystals, electromagnetically induced transparency*.

1. Introduction

The study of photonic crystals and the fabrication of devices based on them is at present a new extensively developed direction in optics [1 – 4]. Photonic crystals uniquely combine dispersion properties and localisation of radiation, allowing the efficient control of light beams. New possibilities appear in the so-called resonance photonic crystals, in which their intrinsic spectral and dispersion properties are supplemented by the properties of impurity atoms [5, 6] and quantum wells [7, 8] embedded into them.

Such structures feature unusual linear and nonlinear optical properties and are of interest not only from the physical point of view but also because they can be used for the development of optical devices, for example, microtransistors and switches [5], optical memory [9], etc.

Media possessing electromagnetically induced transparency (EIT) feature unique properties (see, for example, review [10]). We will call a material in which EIT can be observed an EIT medium. In the case of EIT, a resonantly absorbing medium becomes transparent for a probe pulse and strongly dispersive in the presence of an additional strong laser field. Electromagnetically induced transparency is related to a number of phenomena such as the group-velocity delay of light pulses ('slow' light) [11], the writing, storage, and reading of information about light pulses [12, 13], the effective nonlinear interactions of low-energy laser pulses, including single-photon pulses [14], etc. These effects were observed in atomic media and solids doped with rare-earth ions, in N-V centres in diamond, a Bose – Einstein condensate and semiconductor quantum wells [10]. Interesting effects appear when an EIT medium is introduced inside an optical cavity. In particular, a considerable narrowing (approximately by two orders of magnitude) of the transmission band of a travelling-wave cavity filled with an EIT medium was observed compared to the transmission band of an empty cavity [15 – 17].

The combination of the properties of an EIT medium with the properties of photonic crystals opens up new possibilities for controlling the optical properties of photonic crystals and light [18 – 22]. In this respect, of great interest are photonic crystals containing micro- or nanodefects – micro- and nanocavities. Such structures can localise light in a volume smaller than λ^3 (λ is the light wavelength) [23]. As a result, low-power radiation (and even single photons) can strongly interact with matter [18]. It was shown in [19] that the introduction of an EIT medium as a defect into a photonic crystal leads to the increase in the lifetime of a defect mode (increase in the Q factor). In [20], an optical switch based on this effect was proposed with the switching power corresponding to a few tens of photons and the switching time ~ 100 ps. It was assumed in these papers that the spatial size of the EIT medium is much smaller than the light wavelength.

Undoubtedly, of interest is the case when the size of the region occupied by the EIT medium is comparable with the light wavelength. In this case, it should be taken into account that photonic-crystal modes are spatially inhomogeneous because EIT depends on the control-field intensity at a given point. This circumstance motivates the further study of the optical properties of photonic crystals combined with EIT media. The aim of our paper is to study the spectral properties of a one-dimensional photonic crystal containing an EIT defect layer of thickness comparable with the light wavelength. The analysis is performed taking into account the spatial inhomogeneity of fields inside the defect layer. Two cases are considered: (i) the frequencies of the interacting fields are close and, therefore, defect modes excited by the fields are well spatially overlapped; and (ii) the frequencies of the fields are well separated, so that defect modes excited by them have different spatial distributions.

V.G. Arkhipkin, S.A. Myslivets L.V. Kirenskii Institute of Physics, Siberian Branch, Russian Academy of Sciences, Akademgorodok, 660036 Krasnoyarsk, Russia; Siberian Federal University, prosp. Svobodnyi 79, 660041 Krasnoyarsk, Russia;
e-mail: avg@iph.krasn.ru, sam@iph.krasn.ru

Received 5 February 2008; revision received 8 May 2008
Kvantovaya Elektronika **39** (2) 157 – 162 (2009)
Translated by M.N. Sapozhnikov

2. The model and its approximations

Consider a one-dimensional photonic crystal of structure of the type $(HL)^M HDH(LH)^M$ (Fig. 1). Here, H and L denote dielectric layers with the high and low refractive indices n_H and n_L and thicknesses d_H and d_L; $t = d_H + d_L$ is the structure period; M is the number of bilayers (periods); and D is a defect layer with the refractive index n_D and thickness d_D. The defect layer is filled with a medium, which we simulate by three-level atoms (Fig. 2), assuming that they are at rest and do not interact with each other. Transitions between the lower ground state $|0\rangle$ and the metastable $|2\rangle$ state are dipole forbidden. Only the $|0\rangle$ state is initially populated.

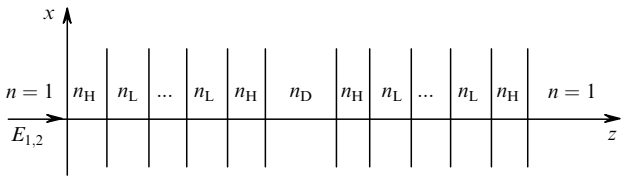

Figure 1. Schematic structure of a one-dimensional photonic crystal with a defect layer.

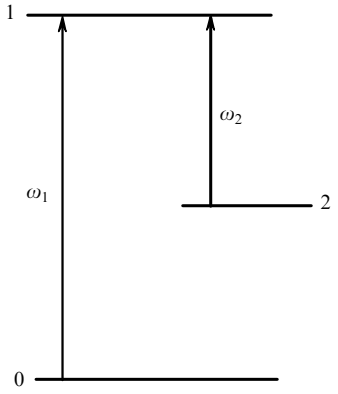

Figure 2. Energy level diagram of a three-level atom interacting with a weak probe (frequency ω_1) and a strong control (frequency ω_2) laser fields.

Electromagnetically induced transparency appears due to the interaction of a three-level atom with two laser fields: a weak probe field with frequency ω_1 and a strong control field with frequency ω_2, as shown in Fig. 2. The refractive index for the probe field $n_p = n_D$ in the presence of the strong control field interacting with an adjacent transition has the form [10]:

$$n_D = 1 + \frac{1}{2}\chi = 1 + F\frac{\Gamma_{10}\Delta_{20}}{\Delta_{20}\Delta_{10} + |G_2|^2}, \qquad (1)$$

where χ is the macroscopic susceptibility of atoms to the probe field; $\Delta_{10} = \omega_1 - \omega_{10} - i\Gamma_{10}$; $\Delta_{20} = \omega_1 - \omega_2 - \omega_{20} - i\Gamma_{20}$; ω_{10}, ω_{20} and Γ_{10}, Γ_{20} are the resonance frequencies and half-widths of the corresponding transitions, respectively; G_2 is the Rabi frequency for the control field; $F = |d_{10}|^2 N/(2\hbar\varepsilon_0\Gamma_{10})$; d_{10} is the matrix dipole moment of the $|1\rangle - |0\rangle$; transition; $\hbar$ is Planck's constant; ε_0 is the dielectric constant; and N is the density of atoms. The field distribution in the defect in the photonic crystal is inhomogeneous, and therefore the Rabi frequency of the control field depends on the spatial coordinate z, i.e. $G_2 = G_2(z)$. For $G_2 = 0$ (the control field is absent), expression (1) describes the usual linear refractive index.

Figure 3 shows the dependences $\mathrm{Re}\,\chi$ (addition to the refractive index) and $\mathrm{Im}\,\chi$ (absorption) for an ensemble of atoms with Lorentzian shapes of the allowed-transition lines on the normalised detuning of the probe field frequency $\Omega_1 = (\omega_1 - \omega_{10})/\Gamma_{10}$ for the case of the resonance control field. One can see that the absorption spectrum for probe radiation has a narrow dip (the transparency window) corresponding to a decrease in the absorption of radiation at the frequency satisfying the two-photon (Raman) resonance $\omega_1 - \omega_2 - \omega_{20} = 0$. The width of the transparency window can be much smaller the linewidth of the allowed $|0\rangle - |1\rangle$ transition. The effect can be observed if the Rabi frequency of the control radiation inducing the Stark (dynamic) splitting of the level $|1\rangle$ exceeds Γ_{10}. The spectral dependence of the refractive index has a steep slope in the transparency window region, corresponding to a large dispersion. Note that the higher the control field intensity, the greater the depth and width of the dip. Such a behaviour of the refractive index for the probe wave is caused by the quantum coherence and interference of different channels of the transition of atoms from the $|0\rangle$ state to the $|1\rangle$ state [10]. Figure 3 also shows for comparison similar dependences for the resonance susceptibility in the absence of the control voltage.

Consider two plane monochromatic waves $E_{1,2}$ with frequencies $\omega_{1,2}$ incident normally on a photonic crystal and propagating along the z axis ($z = 0$ corresponds to the boundary of the first layer). In the stationary approximation, the wave equation describing the propagation of waves in the photonic crystal has the form [1]

$$\frac{d^2 E_{1,2}}{dz^2} + \frac{\omega_{1,2}^2 n^2(z,\omega)}{c^2} E_{1,2} = 0, \qquad (2)$$

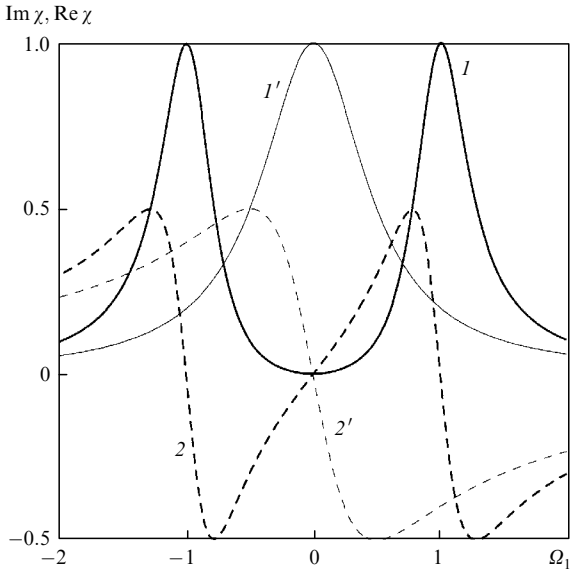

Figure 3. Dependences of normalised imaginary (*1*, *1′*) and real (*2*, *2′*) components of the EIT susceptibility (*1*, *2*) ($G_2 = \Gamma_{10}$, $\omega_2 - \omega_{12} = 0$, $\Gamma_{10}/\Gamma_{20} = 10$) and of the usual linear resonance susceptibility (*1′*, *2′*) ($G_2 = 0$) on the probe-field frequency detuning.

where c is the speed of light in vacuum; n is the refractive index equal to $n_{\rm H}$, $n_{\rm L}$ or $n_{\rm D}$ in the corresponding layer for the probe and control waves (dispersion of $n_{\rm H}$ and $n_{\rm L}$ is neglected).

Each field in the jth layer (j corresponds to one of the layers H, L, D) is a superposition of the forward and backward waves representing the solution of equation (2):

$$E_{1j,\,2j}(z) = A_{1j,\,2j}\,{\rm e}^{{\rm i}q_{1j,\,2j}z} + B_{1j,\,2j}\,{\rm e}^{-{\rm i}q_{1j,\,2j}z}. \tag{3}$$

Here, $A_{1j,\,2j}$ and $B_{1j,\,2j}$ are the amplitudes of the forward and backward waves; $q_{1j,\,2j} = k_{1,2}n_j$; $k_{1,2} = 2\pi/\lambda_{1,2}$; and n_j is the refractive index for the corresponding wave in the jth layer.

The amplitudes $A_{1j,\,2j}$ and $B_{1j,\,2j}$ can be conveniently calculated by using the method of recurrent relations [24, 25]. For this purpose, we divide all the photonic-crystal layers into a sufficiently large number K of sublayers such that the field can be assumed constant within each sublayer with the number m. By using the continuity conditions for the electric and magnetic components of the fields at the interface of sublyers with numbers m and $m+1$, we obtain the system of equations connecting the field amplitudes in adjacent sublayers (hereafter, subscripts 1 and 2 are omitted):

$$A_m + B_m = g_{m+1}^{-1}A_{m+1} + g_{m+1}B_{m+1}, \tag{4}$$

$$q_m(A_m - B_m) = q_{m+1}(g_{m+1}^{-1}A_{m+1} - g_{m+1}B_{m+1}), \tag{5}$$

where $g_m = \exp({\rm i}q_m t_m)$; $m = 1, 2, ..., K+1$; $t_m = z_{m+1} - z_m$ are the thickness of sublayers; and the thickness of the last sublayer is $t_{K+1} \equiv 0$. The functions g_m take into account variations in the phases of the waves and their decay in the mth sublayer.

By introducing the amplitude reflection coefficients $R_m = B_m/A_m$, we can obtain the recurrent relation from (4) and (5), which connects the coefficients R_m and R_{m+1} in the adjacent sublayers:

$$R_m = \frac{r_m + g_{m+1}^2 R_{m+1}}{1 + r_m g_{m+1}^2 R_{m+1}}. \tag{6}$$

Here, $r_m = (q_m - q_{m+1})/(q_m + q_{m+1})$. By using relation (6), we find all R_m, beginning from the right boundary of the photonic crystal, taking into account the boundary condition $R_{K+1} = 0$, and express A_{m+1} in terms of A_m in an arbitrary sublayer m:

$$A_{m+1} = A_m \frac{1 + R_m}{g_{m+1}^{-1} + g_{m+1}R_{m+1}}. \tag{7}$$

By using relation (7), we determine all A_m, beginning from the left boundary of the photonic crystal. Then, we calculate the amplitude of the backward wave $B_m = A_m R_m$. The transmission (T) and reflection (R) coefficients for the probe wave are determined by the relations

$$T = |A_{1\,K+1}|^2/|A_{10}|^2, \quad R = |B_{10}|^2/|A_{10}|^2. \tag{8}$$

Here, A_{10} and $A_{1\,K+1}$ are the amplitudes of the probe wave at the input and output of the photonic crystal, and B_{10} is the amplitude of the probe wave reflected from the input face of the photonic crystal. The spatial distribution of the control field is calculated for $n_{\rm D} = 1$ and is assumed given in the calculation of the transmission coefficient for the probe wave.

3. Results and discussion

By using the expressions presented above, we calculated the transmission and spatial distribution of the amplitudes of the probe and control waves under different conditions. It was assumed that the probe wave is weak ($|E_1| \ll |E_2|$) and does not change the population of levels. Therefore, we calculated the transmission of the probe field under the EIT conditions by assuming that the control field has the given spatial distribution inside the photonic crystal, which is established in the absence of the probe wave for the specified parameters.

3.1 The case of close frequencies

In this case, the difference between the frequencies of the probe and control fields is smaller than the width of the defect mode of the photonic crystal. As the EIT medium, we considered sodium atoms, which are often used in EIT experiments (see, for example, [26]). The probe radiation wavelength corresponds to the transition near the 589.6-nm D_1 line of sodium, while the $|0\rangle$ and $|2\rangle$ levels are close to each other [$(\omega_{10} - \omega_{12})/2\pi = 1.8$ GHz]. The photonic-crystal parameters were: $M = 10$, $n_{\rm H}d_{\rm H} = n_{\rm L}d_{\rm L} = \lambda_1/4$, $d_{\rm D}n_{\rm D} = \lambda_1/2$, $n_{\rm H} = 2.35$, $n_{\rm L} = 1.45$, $\lambda_1 = 589.6$ nm corresponds to the centre of the band gap, and a defect is located at the photonic-crystal centre.

The solid curve in Fig. 4 shows the transmission spectrum of the photonic crystal for the probe wave in the absence of resonance atoms ($n_{\rm D} = 1$) in the defect layer. The spectrum represents a sharp peak at the resonance wavelength $\lambda_{\rm D} = \lambda_1$, its maximum corresponding to $\Omega_1 = 0$. The parameters of the photonic crystal were selected so the spectrum of the defect mode well overlapped with the atomic $|0\rangle - |1\rangle$ and $|1\rangle - |2\rangle$ transitions (for the Na atom) and its spectral width greatly exceeded the frequency difference of the interacting fields. The dashed curve corresponds to the transmission spectrum of the photonic spectrum for the probe wave in the presence of a resonance two-level medium in the defect layer and in the absence of

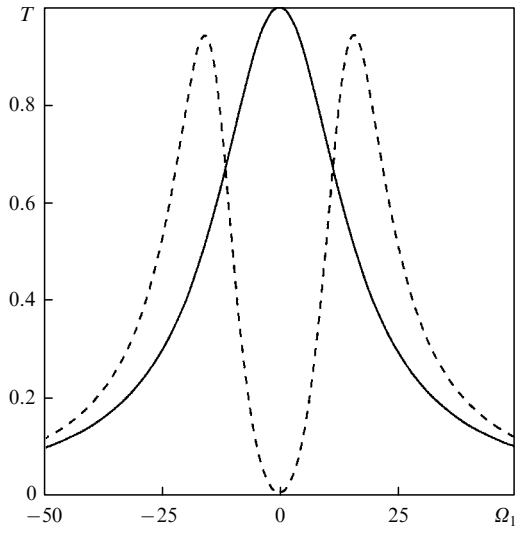

Figure 4. Transmission spectra of the photonic crystal for the probe wave in the absence of resonance atoms in the defect ($n_{\rm D} = 1$) (solid curve) and in their presence in the absence of the control field (dashed curve) for $F = 5 \times 10^{-4}$ and $\omega_2 - \omega_{12} = 0$.

the control laser radiation. One can see that in this case the two peaks are observed with virtually zero transmission at the centre between them. Such a behaviour of the defect mode is caused by linear absorption and dispersion related to resonance atoms in the defect layer [6–8]. This effect can be treated as the splitting of the defect mode of the photonic crystal. It is similar to the appearance of the normal mode of semiconductor microcavities [8]. Note that the interaction of interband excitations with the electromagnetic field in a semiconductor cavity is now being extensively studied [27]. On the other hand, this effect is also identical to the vacuum Rabi splitting of the optical cavity resonance [28].

Figure 5 shows the spatial distribution of the control field intensity in the photonic crystal at the resonance frequency $\omega_2 = \omega_{12}$. One can see that the field is localised in the defect layer. Because of the closeness of frequencies, the spatial distribution of the probe field at the resonance frequency $\omega_1 = \omega_{10}$ in the presence of the control field virtually coincides with the spatial distribution of the latter. Due to localisation, these fields considerably exceed their values at the input to the photonic crystal.

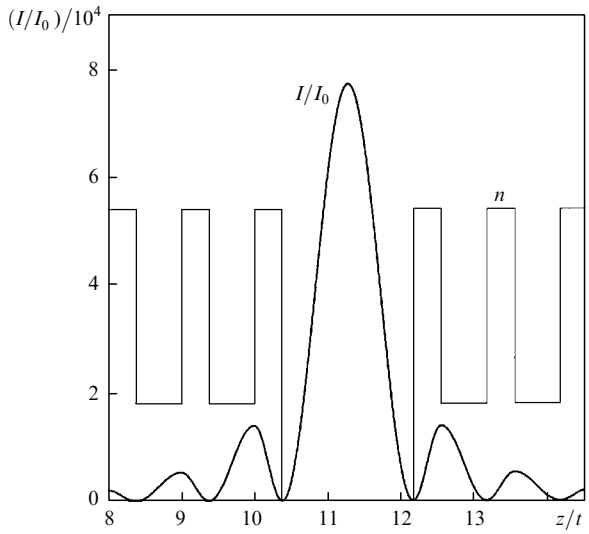

Figure 5. Spatial distribution of the control-field intensity inside the photonic crystal (heavy curve) and schematic refractive-index profile (thin curve). The length z is normalised to the structure period t and the intensity is normalised to the input intensity I_0.

Figure 6 presents the transmission spectrum of the photonic crystal for the probe wave under the EIT conditions in the defect layer for different control-radiation intensities. It was assumed in calculations that the control field has the spatial distribution shown in Fig. 5. One can see that a narrow peak is observed at the centre of the transmission line, which is caused by the nonabsorbing strongly dispersive resonance taking place under EIT conditions. The spectral width of this peak is much smaller than the width of a usual (nonresonance) defect mode. This peak is the manifestation of the EIT effect. Two other peaks are similar to the peaks shown by the dashed curves in Fig. 4. The values of the Rabi frequency (Fig. 6) correspond to the control-field intensity (at the photonic-crystal input) of a few mW cm^{-2}, which is comparable to intensities at which EIT was observed in usual cells (see, for example, [9, 26]) or even smaller. Note that, as the ratio Γ_{10}/Γ_{20} increases, the control-field intensity required for observing EIT decreases. In this case, the central maximum narrows down. The field localisation effect also allows the observation of EIT in media small oscillator strengths (for example, in rare-earth ions), when high-intensity control fields are required. The position of the central resonance can be changed by varying the control-field frequency. Figure 7 shows the transmission spectrum of the photonic crystal for the case when the control-radiation frequency is detuned from the resonance. One can see that the narrow resonance shifts and broadens.

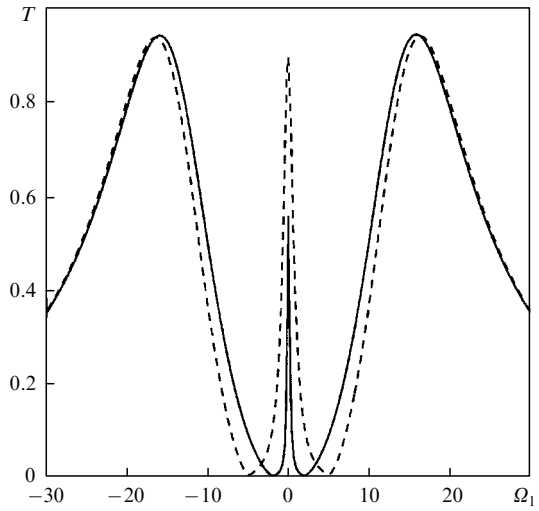

Figure 6. Transmission spectra of the photonic crystal for the probe wave under EIT conditions for $G_2 = 2\Gamma_{10}$ (solid curve) and $5\Gamma_{10}$ (dashed curve) (the values of G_2 correspond to the maximum control-field intensity); $\Gamma_{10}/\Gamma_{20} = 10$, $F = 5 \times 10^{-4}$.

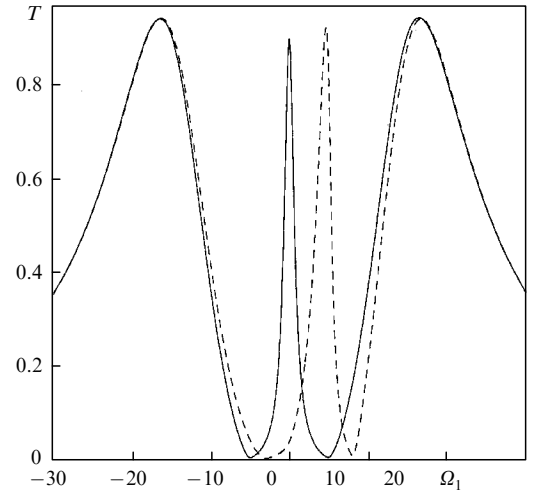

Figure 7. Transmission spectra of the photonic crystal for the probe wave under EIT conditions for $\omega_2 - \omega_{12} = 0$ (solid curve) and $5\Gamma_{10}$ (dashed curve); $G_2 = 5\Gamma_{10}$ correspond to the maximum control-field intensity.

3.2 The case of well-separated frequencies

In this case, the frequency difference of the interacting fields exceeds the spectral width of the defect mode, and the frequencies of the probe and control waves do not fall

simultaneously into the transparency window of the photonic crystal. Therefore, it is necessary to have two defect modes. In this case, the spatial distributions of the fields of different defect modes will be different, which considerably influences the effect under study. Consider a photonic crystal with parameters $M = 35$, $n_D d_D = 3\lambda_0/4$ (λ_0 corresponds to the centre of the first forbidden zone), other parameters having the same values as in the previous case. Such a photonic crystal has two defect modes with spectra located near the edges of the forbidden photonic zone. The mode at the control-field frequency is located near the long-wavelength edge of the zone, while at the probe-field frequency – near the short-wavelength edge of the zone. Let us assume that the difference of these frequencies is equal to the frequency of the $|0\rangle - |2\rangle$ transition in a hypothetical EIT medium.

Figure 8 shows spatial distributions of the intensity of defect modes excited by the probe and control wave in the defect region. One can see that the maxima of the distributions do not coincide (the probe field oscillates two times in the defect region). The calculated transmission spectrum for the probe wave under EIT conditions is shown in Fig. 9a, where the spectrum of the defect mode for the probe field in the absence of the control field is also shown for comparison. The dip at the centre corresponds to the splitting of the defect mode excited by the probe field (as in Fig. 4). Unlike the case of close frequencies, in this case the transmission spectrum of the photonic crystal under EIT conditions has a more complicated form, exhibiting a narrow peak located on a broad 'pedestal', whose width and height depend on the control-field intensity. We explain such behaviour of the transmission spectrum by the specific features of the spatial distribution of the interacting fields.

The behaviour of the photonic-crystal transmission under EIT conditions can be explained qualitatively by using analogy between a one-dimensional photonic crystal with a defect and a Fabry–Perot resonator of length d equal to the thickness of the defect layer in the photonic crystal and filled with a EIT medium. In the case of identical

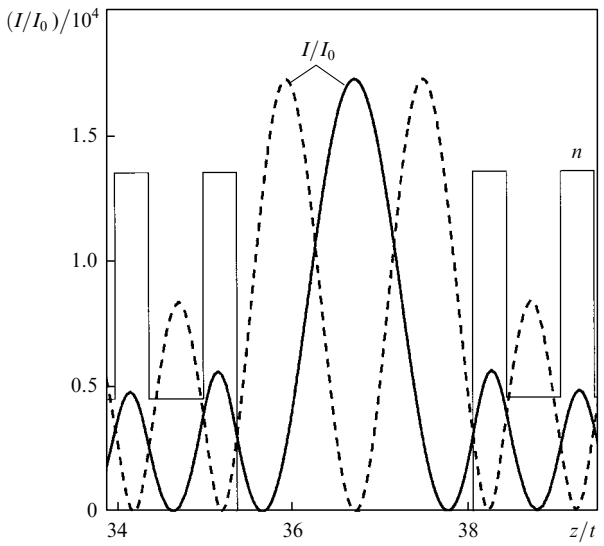

Figure 8. Spatial distributions of the probe (dashed curve) and control (heavy curve) waves and the schematic refractive-index profile (thin curve).

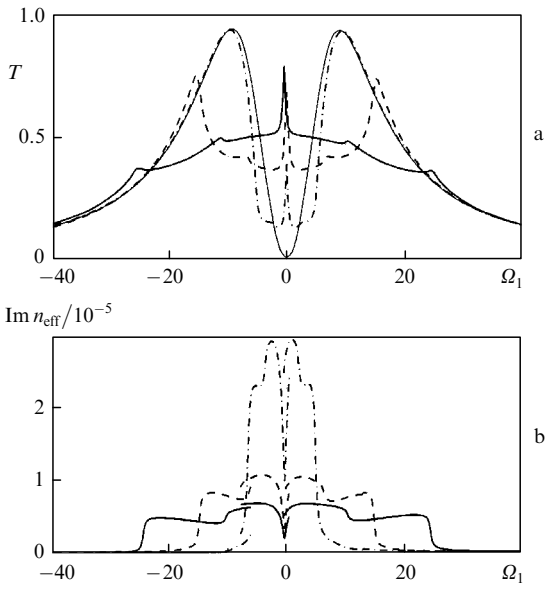

Figure 9. Transmission spectra of the photonic crystal for the probe wave under EIT conditions (a) and dependences of the effective refractive index on the frequency detuning of the probe wave (b) for $G_2 = 25\Gamma_{10}$ (heavy curves), $15\Gamma_{10}$ (dashed curves), $5\Gamma_{10}$ (dot-and-dash curves) and $G_2 = 0$ (thin curve); $\omega_2 - \omega_{12} = 0$, $\Gamma_{10}/\Gamma_{20} = 10$.

mirrors, the transmission coefficient of the resonator $T = I_t/I_0$ (I_0 is the light intensity at the input to the Fabry–Perot resonator, I_t is the transmitted light intensity) is determined by the Airy formula [29]

$$T = \frac{T_m^2}{|1 - R_m \exp(\mathrm{i}\delta)|^2}, \tag{9}$$

where T_m and R_m are the transmission and reflection coefficients of mirrors ($T_m + R_m = 1$) and δ is the round-trip transit phase shift. Note that T_m and R_m are dependent in the general case on the light wavelength. Because the fields in the resonator are inhomogeneous, by using the method of the field expansion in the resonator modes applied in the theory of lasers [30], we can easily show that the phase shift δ, taking EIT into account, is determined by the expression (in the case of normal incidence)

$$\delta = \frac{4\pi d}{\lambda}(1 + \chi_{\mathrm{eff}}) = \frac{4\pi d n_{\mathrm{eff}}}{\lambda}. \tag{10}$$

Here

$$\chi_{\mathrm{eff}} = \frac{1}{d}\int_0^d U_1(z)\chi(z)dz;$$

$U_1(z)$ is a normalised resonator mode excited by the probe field and $\chi(z)$ is the EIT susceptibility from (1). The parameter χ_{eff} can be treated as the effective EIT susceptibility calculated with the weight factor $U_1(z)$.

It follows from (9) and (10) that all the features of the behaviour of the transmission coefficient for the probe field are determined by the effective susceptibility χ_{eff} or the effective refractive index n_{eff}. Figure 9b presents the dependences of $\mathrm{Im}\, n_{\mathrm{eff}}$ on the probe-field frequency for different control-radiation intensities, which explain the behaviour of transmission.

One can see that the shape of the effective absorption line $\mathrm{Im}\, n_{\mathrm{eff}}$ is quite unusual, and the line amplitude decreases and its width increases with increasing the control-field

intensity. This can be explained by considering the spectral distribution of $\mathrm{Im}\, n(z)$ inside the defect layer presented in Fig. 10. In the regions where the control field is zero, the line of the transition interacting with the probe field splits. The splitting value depends on the control-field strength at the given point. Splitting disappears in the region where the field amplitude vanishes and achieves maximum at the defect centre (see Fig. 8). The dependence $\mathrm{Im}\, n(z)$ at the resonance frequency ($\Omega_1 = 0$) has two narrow peaks at $z/t = 35.7$ and 37.8, and absorption integrated over the defect length is minimal, which is manifested as a narrow peak in the transmission spectrum. As the detuning is increased up to $\Omega_1 \approx 2$ (see Fig. 10), four peaks appear in the dependence $\mathrm{Im}\, n(z)$ and the integrated absorption increases, weakly changing in this spectral region. As the detuning is further increased, two peaks remain in the dependence $\mathrm{Im}\, n(z)$, resulting in the stepwise decrease in the integrated absorption and appearance of additional resonances in the transmission spectrum. When detunings exceed the line splitting in the field, the transmission spectrum remains almost the same as in the absence of the control field (shown by the thin solid curve in Fig. 9a).

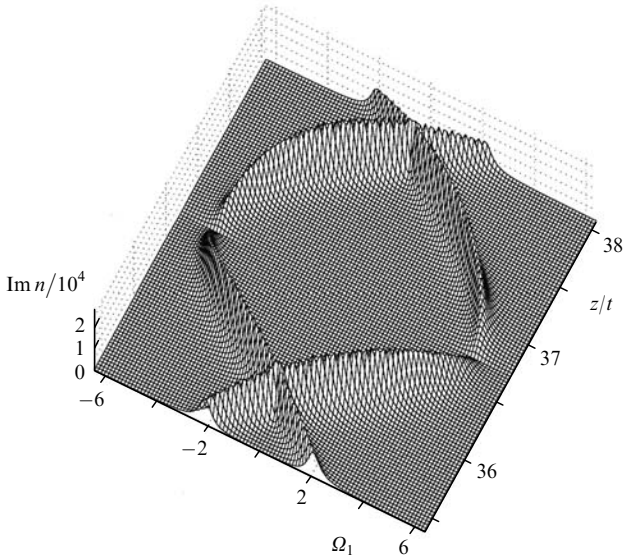

Figure 10. Spectral distribution of $\mathrm{Im}\, n(z)$ inside the defect layer for $G_2 = 5\Gamma_{10}$.

4. Conclusions

We have studied theoretically the transmission spectrum of a one-dimensional photonic crystal containing a defect EIT-medium layer of thickness comparable with the light wavelength. Calculations performed taking into account the spatial distributions of the control and probe fields show that EIT can considerably reduce the spectral width of the defect mode of the photonic crystal for probe radiation. In this case, the control-radiation intensity is comparable with the radiation intensity in the case of a usual cell, in which EIT is observed, or lower than it. The position of the transmission maximum of the photonic crystal with the defect layer can be changed by varying the control-field frequency. The shape of the transmission spectrum depends on the spatial distributions of the probe and control fields in the photonic crystal and is determined by the spatially-integrated refractive index of the defect layer. The field localisation allows the observation of EIT in media with low oscillator strengths, when high-intensity control fields are required. The narrow resonance in the transmission spectrum can be used to reduce the group velocity of the probe pulse.

Acknowledgements. This work was supported by Grants NSh-3818.2008.3, DSP.2.1.1.1814 and Integration Project No. 33 SB RAS.

References

1. Shabanov F.V., Vetrov S.Ya., Shabanov A.V. *Optika real'nykh fotonnykh kristallov: zhidkokristallichesie defekty, neodnorodnosi* (Optics of Real Photonic Crystals: Liquid-crystal Defects and Inhomogeneities) (Novosibirsk; Izd. SB RAS, 2005).
2. Busch K., von Freymann G., Linden S., et al. *Phys. Rep.*, **444**, 101 (2007).
3. Russell P. *Science*, **299**, 358 (2003).
4. Zheltikov A.M. *Usp. Fiz. Nauk*, **174**, 1301 (2004) [*Phys. Usp.*, **47**, 1205 (2004)].
5. John S., Florescu V. *J. Opt. A: Pure Appl. Opt.*, **3**, S101 (2001).
6. Arkhipkin V.G., Myslivets S.A., Timofeev I.V., et al. *Proc. Conf. LFNM 2006* (Kharkiv, Ukraine, 2006) p. 313.
7. Ivchenko E.L., Kaliteevski M.A., Kavokin A.V., et al. *J. Opt. Soc. Am. B*, **13**, 1061 (1996).
8. Khitrova G., Gibbs H.M. *Rev. Mod. Phys.*, **71**, 1591 (1999).
9. Zhou O., Shao H., Yu X. *Opt. Lett.*, **30**, 1560 (2005).
10. Fleischhauer M., Immamoglu A., Marangos J.P. *Rev. Mod. Phys.*, **77**, 633 (2005).
11. Matsko A.B. et al. *Adv. At., Mol., Opt. Phys.*, **46**, 191 (2001).
12. Lukin M.D., Immamoglu A. *Nature*, **412**, 273 (2001).
13. Arkhipkin V.G., Timofeev I.V. *Pis'ma Zh. Eksp. Teor. Fiz.*, **76**, 74 (2002) [*JETP Lett.*, **76**, 66 (2002)].
14. Harris S.E., Hau L.V. *Phys. Rev. Lett.*, **82**, 4611 (1999).
15. Muller G., Muller M., Rinkleff R.-Y., et al. *Phys. Rev. A*, **56**, 2385 (1997).
16. Lukin M.D., Fleischhauer M., Scully M.O. *Opt. Lett.*, **23**, 295 (1998).
17. Wang Y., Goorskey D.J., Burkett W.H., et al. *Opt. Lett.*, **25**, 1732 (2000).
18. Soljacic M., Joannopoulos J.D. *Nature Mater.*, **3**, 211 (2004).
19. Soljacic M., Lidorikis E., Hau L.V., et al. *Phys. Rev. E*, **71**, 026602 (2005).
20. Soljacic M., Lidorikis E., Joannopoulos J.D., et al. *Appl. Phys. Lett.*, **86**, 171101 (2005).
21. Rostovtsev Yu.V., Matsko A.B., Scully M.O. *Phys. Rev. A*, **57**, 4919 (1998).
22. Radeonychev Y.V., Erukhimova M.A., Kocharovskaya O.A., et al. *Radiophys. Quantum Electron.*, **47** (10-11), 884 (2004).
23. Vuckovic V., Yamamoto Y. *Appl. Phys. Lett.*, **82**, 2374 (2003).
24. Balakin A.V., Bushuev V.A., Mantsyzov B.I., et al. *Phys. Rev. E*, **63**, 046609 (2001).
25. Arkhipkin V.G., Gunyakov V.A., Myslivets S.A., et al. *Zh. Ekp. Teor. Fiz.*, **133**, 447 (2008) [*JETP*, **106**, 388 (2008)].
26. Hau L.V., Harris S.E., Dutton Z., et al. *Nature*, **397**, 594 (1999).
27. Anappara A., Tredicucci A., et al. *Apll. Phys. Lett.*, **87**, 051105 (2005).
28. Zhu Y., Gauthier D.J., et al. *Phys. Rev. Lett.*, **64**, 2499 (1990).
29. Demtroder W. *Laser Spectroscopy: Basic Concepts and Instrumentation* (New York: Springer-Verlag, 1981; Moscow: Nauka, 1985).
30. Stenholm S. *Fundamentals of Laser Spectroscopy* (New York: Wiley, 1984; Moscow: Mir, 1987).